Plasma Chem Plasma Process (2016) 36:901–915
DOI 10.1007/s11090-016-9718-1

ORIGINAL PAPER

Operando DRIFT Spectroscopy Characterization of Intermediate Species on Catalysts Surface in VOC Removal from Air by Non-thermal Plasma Assisted Catalysis

Anthony Rodrigues[1] · Jean-Michel Tatibouët[1] · Elodie Fourré[1]

Received: 3 February 2016 / Accepted: 11 May 2016 / Published online: 20 May 2016
© Springer Science+Business Media New York 2016

Abstract An innovative plasma discharge reactor was developed to fit an infrared cell and to allow the in situ characterization of isopropanol (IPA) and toluene decomposition at the surface of three metal oxides (γ-Al_2O_3, TiO_2 and CeO_2). The impact of the plasma discharge on the conversion of these pollutants, with the material placed in the discharge area, was studied under real time conditions at atmospheric pressure via infrared analysis. The plasma treatment of IPA molecules led to the formation of acetone, propene, acetic acid and/or formic acid. By contrast, the toluene oxidation led to the rapid opening of the aromatic ring, followed by the total oxidation through carboxylic formation of the species arising from the toluene molecules fragmentation.

Keywords In-situ characterization · Infrared spectroscopy · Non-thermal plasma · VOC

Introduction

Non thermal atmospheric plasma (NTAP) is now recognized as an innovative technology applied to a wide range of applications (etching, deposition of thin film, volatile organic compound oxidation, surface functionalization, biomedical…) [1]. The advantageous properties of NTAP, in terms of energetic and environmental aspects, are responsible for the enhanced research in this field. Non thermal atmospheric plasmas are produced by a variety of electrical discharges or electron beams leading to plasmas such as corona discharges, gliding arc discharges, dielectric barrier discharges (DBD), plasma needle, plasma jets and micro hollow cathode discharges [2]. Non thermal plasmas are generated by the

✉ Elodie Fourré
elodie.fourre@univ-poitiers.fr

[1] Institut de Chimie des Milieux et Matériaux de Poitiers (IC2MP), UMR CNRS 7285, Ecole Nationale Supérieure d'Ingénieurs de Poitiers (ENSIP), Université de Poitiers, 1, rue marcel Doré, TSA 41105, 86073 Poitiers Cedex 9, France

application of a high potential difference between two electrodes that leads to a strong electrical field, resulting in the formation of a highly reactive environment favorable to various reactions. For decades, non-thermal atmospheric plasma was used mainly for the production of ozone and water purification [3]. More recently, due to a greater concern on environmental issues, research on waste gas treatment, volatile organic compounds (VOCs) removal has been largely studied. In particular, the presence of a catalyst in the plasma discharge resulted in a synergistic effect and improved VOCs conversion [4–6]. However, if research has shown tremendous results on VOCs conversion, a few points remain unclear. It concerns essentially the interactions between the chemical species generated in the plasma discharge and a material surface. The willingness to identify active species in the plasma discharge is very challenging. It is a complex field of research, as the species concentration, nature and energetic power are dependent of the plasma reactor configuration, chemical and electrical parameters. Already, research has been dedicated to in situ identification of plasma species in the gaseous phase by spectroscopic methods [7–15]. Most of these studies are dealing with the characterization of the plasma species but not with their reactivity. Rivallan et al. [11] have studied the evolution of air/CO_2 gas mixture under non-thermal plasma by in situ FTIR at the microsecond time-scale. They showed that the mechanism of CO_2 consumption is reversible and that CO_2 molecules are excited through a collision with excited N_2 molecules, where the transfer of energy occurs by a resonant effect. Other authors tried to elucidate some aspects of the ion chemistry occurring in dielectric barrier and corona discharges with benzene/air [7] or different gases such as gas mixtures including Ar, H_2, N_2, O_2 and CH_4 as plasma precursors [8]. OH radical concentration was determined by indirect detection with salicylic acid [13] and direct measurement by laser-induced fluorescence [12]. Kim et al. [15] have reviewed recent progresses in understanding the interaction of NTP and catalysts. They insisted on the effects of the electrical characteristics of the catalyst on the plasma discharge generation and therefore chemical reactivity. In a recent publication [14], we have shown that the decomposition of isopropanol (IPA) by non-thermal plasma on γ-Al_2O_3, analyzed by operando Fourier Transform Infrared (FTIR) under low vacuum could proceed via oxidation, aldolization and fragmentation mechanisms. Such cascade reactions were only possible when γ-Al_2O_3 catalyst was placed in the discharge zone. This VOC has been studied and published in the literature with results essentially based on the analysis of the outlet gas composition. IPA conversion leads to the formation of acetone, acetic acid, formaldehyde (when the reaction is incomplete), formic acid, CO_2 and H_2O [14–19]. Al-Abduly and Christensen [20] reported a spectroscopic study of non-thermal plasma in an air-fed dielectric barrier discharge plasma jet. In situ analysis of the plasma glow and downstream gas by FTIR revealed the presence of various species such as O_3, N_2O_5, N_2O, HNO_3, CO_2, CO and a vibrationally excited form of CO_2 [i.e. CO^*_2 (v)].

Here we are dealing with a non-thermal plasma reactor set at atmospheric pressure and coupled to reflectance infrared spectroscopy. The test reactions studied in this work concerned the removal of isopropanol and toluene from γ-Al_2O_3, TiO_2 and CeO_2 surfaces by non-thermal plasma. The impact of the plasma discharge on the conversion of these pollutants, with the material placed in the discharge area, was studied under real time conditions at atmospheric pressure via infrared analysis.

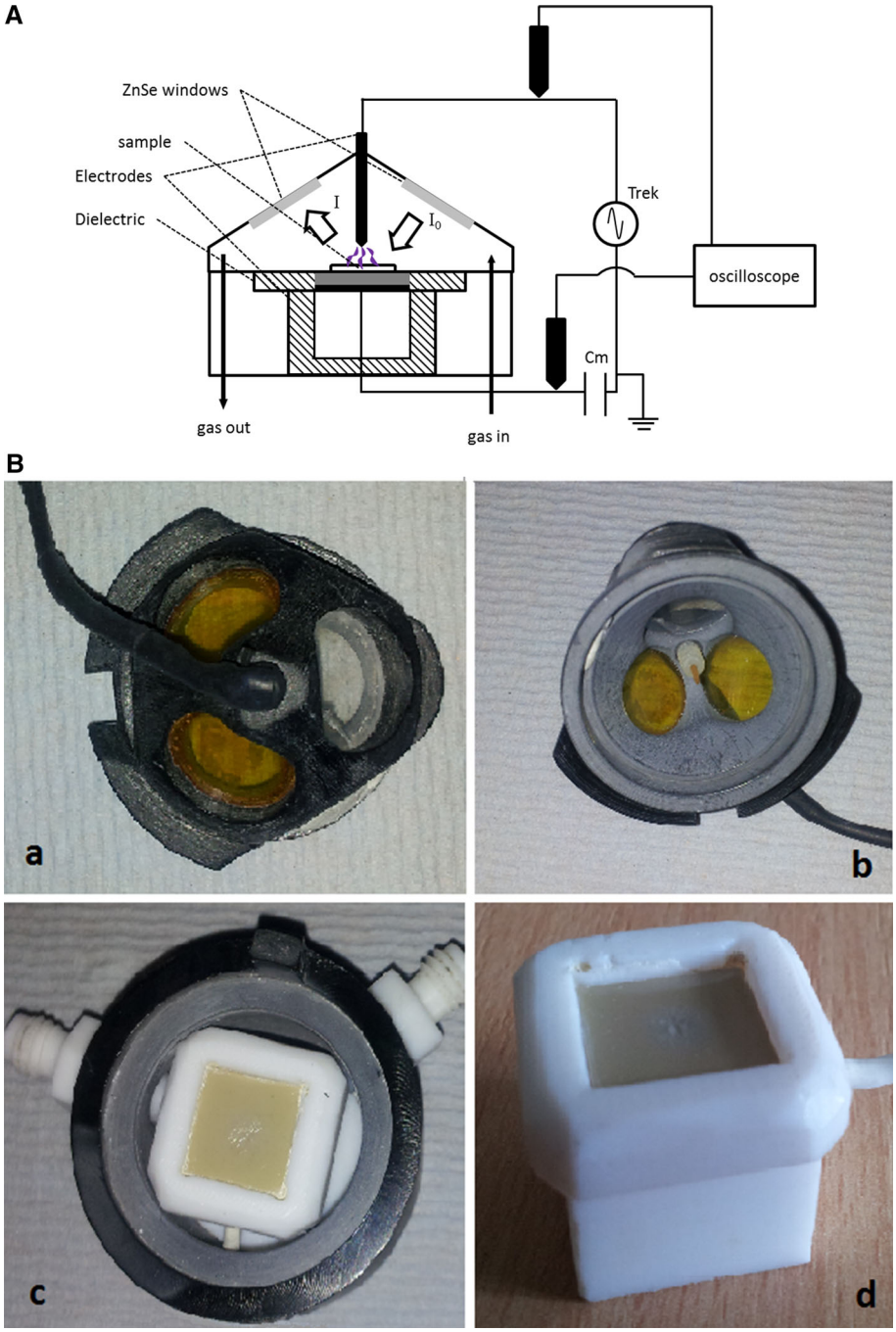

Fig. 1 **a** Schematic of the IR/plasma cell. **b** Views of the disassembled cell (*a–d*)

Experimental

A non-thermal plasma at atmospheric pressure (NTPAP) reactor was developed and optimized for its combination with a DRIFT spectrometer. The spectrometer was modified in order to carry out a DBD plasma in the DRIFT cell while a direct surface analysis was carried out. The cell was made of Polytetrafluoroethylene (PTFE) and included a cylindrical base (30 mm diameter, 29 mm height) and a conical top (26 mm height). The cone was equipped with two ZnSe windows, to allow the passage of the IR beam, and one glass window (Fig. 1a) to view the discharge. The volumic dielectric barrier discharge plasma consisted in a tip electrode (Fig. 1b, tip diameter 0.5 mm) held in the centre of the cone and a counter electrode (10 mm × 10 mm copper tape) placed under a dielectric (0.5 mm thick in PEEK: polyether ether ketone). The sample was placed on the dielectric, underneath the tip. The gap between the tip and dielectric surface was kept constant (1 mm). The electrodes were connected, via a capacitor of known value ($C_m = 0.56$ nF), to a high voltage power amplifier (Trek, 20/20A) coupled to a function generator (TTi TG1010A). Experiments were carried out in an airtight cell with the possibility to vary the chemical and electrical parameters. FTIR Spectrometer Frontier (PerkinElmer, UK), equipped with a Mercury Cadmium Telluride (MCT) detector, was used to record IR spectra in the 4000–900 cm^{-1} range with a resolution of 8 cm^{-1}. Each spectrum is the accumulation of 50 analyses allowing an acquisition time below 1 min. The contributions of gaseous H_2O and CO_2 were subtracted when scanning. Before each experiment the cell was purged with dry air for 10 min (30 mL min^{-1}) before the initiation of the plasma discharge. IR spectra of the sample wafer were then recorded in reflection mode (DRIFT: Diffuse Reflectance Infrared Fourier Transform) as a function of the duration of DBD plasma. Scans were taken while the plasma treatment was switched on and over a period of time going from 1 min to 8 h. All the experiments were carried out at atmospheric pressure.

The DBD experiments were studied under "dynamic" conditions, a flow rate of 30 mL min^{-1} of gas (dry air, Air liquide) was constantly running in the cell chamber.

The power injected in the reactor was determined by the analysis of the Lissajous figure (Fig. 2) that reports the transferred electrical charge Q_m as a function of the applied

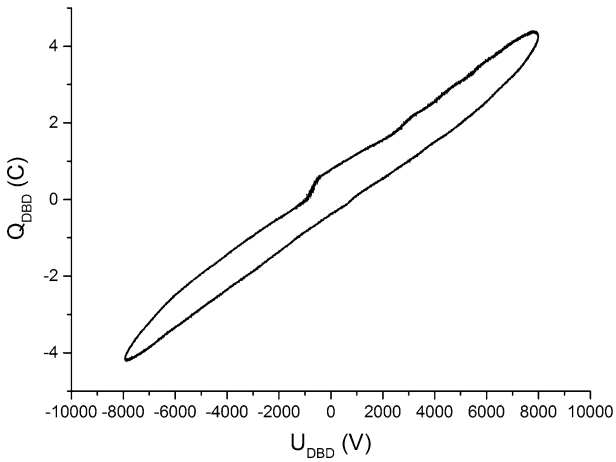

Fig. 2 Lissajous curve at $U_a = 16$ kV and f = 500 Hz

voltage (U_a) using the so-called "Manley method" [21]. Q_m was calculated from the measured voltage (U_m) across the capacitor (C_m) connected in series to the ground electrode. The energy injected, E (per cycle) was calculated from the integration of the area formed by the Lissajous figure. The energy allowed the calculation of the power (in W) injected in the reactor as well as the specific energy E_{spe} (in J L^{-1}) following Eqs. 1 and 2, where f is the frequency (in Hz) and D the gas flow rate in (L s^{-1}):

$$P = E \times f \tag{1}$$

$$E_{spe} = \frac{P}{D} \tag{2}$$

The experiments were carried out at 16 kV (500 Hz), where the plasma discharge was stable, homogeneous and sufficiently energetic to promote excited species. These parameters correspond to a power of 24 mW and an energy density of 48 J L^{-1}.

The catalyst sample was in the form of a thin layer of powder (50–100 mg) slightly pressed on the dielectric plate in order to avoid its spraying under the effect of gas flow rate and plasma. The three oxides were commercial oxides (Table 1). The specific surface area of the samples was determined by the BET (Brunauer–Emmett–Teller) method from the nitrogen adsorption isotherms at −196 °C in an automated Micromeritics Tristar 3000 apparatus after drying for 8 h at 400 °C.

Results

Electrical parameters of the plasma generated in the IR cell were determined with and without the presence of a catalytic material. The influence of the material on the plasma discharge was evaluated by comparing the variation of the plasma power as a function of applied voltage (Fig. 3). A slight decrease of the power is noticed when Al_2O_3 is placed in the discharge, likely due to the slight modification of the dielectric properties of the dielectric plate when covered by alumina.

Isopropanol Removal

All the surfaces were first placed in contact with a gas mixture air/IPA (100 ppm) at atmospheric pressure for 15 min. This was followed by a 10 min flow of air prior to the plasma treatment, also under air flow. Figure 4a displays the evolution of the IR spectra of Al_2O_3 as a function of treatment time, from 1 to 60 min. The same experiment was carried out on the two other oxide surfaces of CeO_2 and TiO_2 (Figs. 5a, 6a). Additionally, spectra of three likely products (acetic acid, formic acid and acetone) were recorded and are displayed in Figs. 4b, 5b and 6b. The spectra were recorded after 10 min adsorption of a mixture of air/product (100 ppm) at atmospheric pressure followed by a 10 min purge under air flow. The IR spectra were obtained after subtraction of the background spectrum

Table 1 Catalysts characteristics

Oxide	Supplier	Surface area (m^2 g^{-1})
γ-Al_2O_3	Degussa	102
TiO_2 P25	Sigma Aldrich	9
CeO_2	Prolabo	23

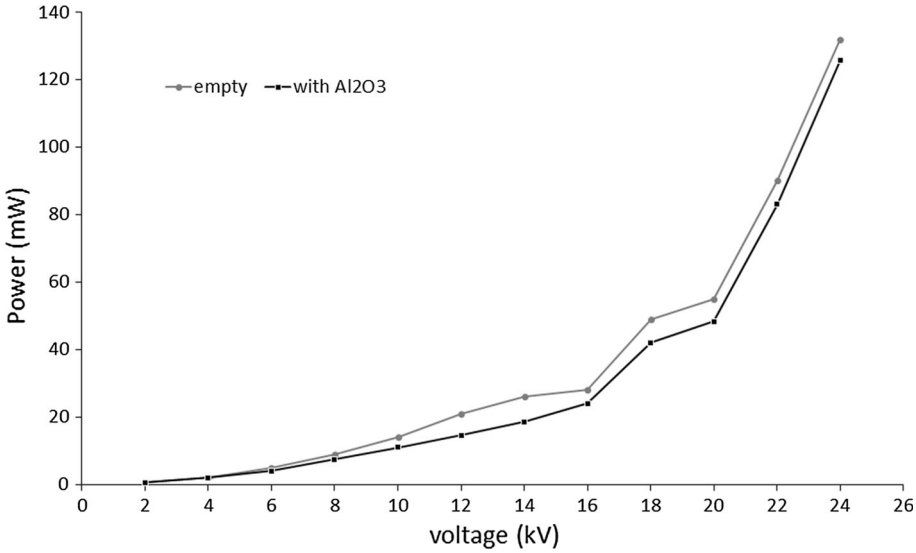

Fig. 3 Injected power in the DBD reactor as a function of the input voltage at atmospheric pressure, under a constant dry air flow of 30 mL min^{-1}

of the sample under air before adsorption. For the three samples, after IPA adsorption and before plasma treatment, the predominant bands corresponding to the C–H asymmetric and symmetric stretching (ν-as and ν-s) were detected between 3030 and 2840 cm^{-1} and between 1510 and 1300 cm^{-1} for the methyl C–H asymmetric and symmetric bends (δ-as and δ-s). Between 1255 and 1205 cm^{-1}, δ–O–H from un-dissociated IPA was identified. Other components, with lower intensity, around 1150 and 1075 cm^{-1} were related to the C–O stretch and C–C skeletal of isopropoxide species, formed via dissociative adsorption of the IPA molecule or/and to molecularly adsorbed IPA [16, 22–25]. The negative bands in the 3750–3600 cm^{-1} region, corresponding to the surface hydroxyl groups of metallic oxides show that IPA adsorption can occur either as isopropoxy group (Scheme 1a) or by coordination with surface OH groups (Scheme 1b).

The remaining negative band even after oxidation of IPA by non-thermal plasma strongly suggests that the IPA is mostly adsorbed as an isopropoxy species (Scheme 1b) rather than by coordination with surface OH groups [26–28]. As soon as the discharge was initiated, the bands corresponding to the methyl group stretching (2975–2840 cm^{-1} region) decreased as a function of the plasma treatment time, whatever the sample. After 60 min of plasma treatment, a residual C–H contribution is still visible which results from the formation of decomposition compounds such as acetone, aldehydes and/or acids. A very broad band going from 3340 to 2250 cm^{-1} emerged after 5 min of treatment for TiO_2 and CeO_2 and 20 min for γ-Al_2O_3 which corresponds to the O–H stretch of carboxylic acid. This band is prominent on γ-Al_2O_3 and similarly, but less evident, on TiO_2 and CeO_2.

In the lower wavenumber region, the analysis is more difficult due to the overlapping of the bands. However, the progressive formation (from 1 to 60 min treatment) of a band corresponding to a C=O group (ketone, aldehyde and/or carboxylic acid) and centered at 1730, 1760 and 1712 cm^{-1} for γ-Al_2O_3, TiO_2 and CeO_2, respectively, is clearly identified. Regarding γ-Al_2O_3 and TiO_2, a shoulder within the ketone region band is visible at a lower

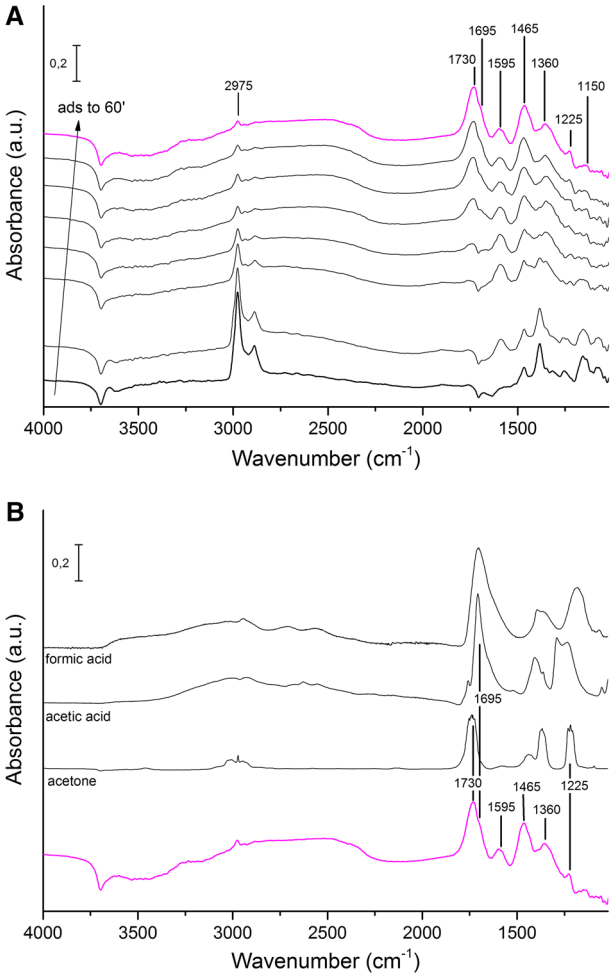

Fig. 4 DRIFT Spectra on γ-Al_2O_3. **a** In situ IR spectra of the evolution of adsorbed isopropanol as a function of plasma treatment time from *bottom* to *top* (adsorbed IPA then 1, 5, 10, 20, 30, 45 and 60 min of plasma treatment). **b** Spectra of adsorbed IPA after 60 min of plasma treatment and adsorbed acetone, acetic acid and formic acid (from *bottom* to *top*)

wavenumber (1695 and 1730 cm^{-1}) and correlates closely to the C=O band of acetic and/or formic acids. CeO_2 presents a much wider band, centered at 1712 cm^{-1}, encompassing the C=O contribution of the acids.

Bands of methyl bending vibrations (δ) evolved differently. On γ-Al_2O_3 surface, an increase and a broadening of the δ-as C–H band (1465 cm^{-1}), a decrease/shift of δ-s C–H band (IPA: 1382 cm^{-1}) to 1360 cm^{-1} were observed as a function of the treatment time. The band at 1360 cm^{-1}, emerging after 5 min, is related to the methyl bending vibrations of acetone [29–31]. The bands at 1595 and 1465 cm^{-1} could be assigned to the C=C stretching and C–H bending mode of methyl or methylene group of propene, respectively [32], according to the products formation observed by IPA oxidation at low temperature on pure γ-Al_2O_3 [33]. Simultaneously, a small shoulder at 1225 cm^{-1} also appeared after

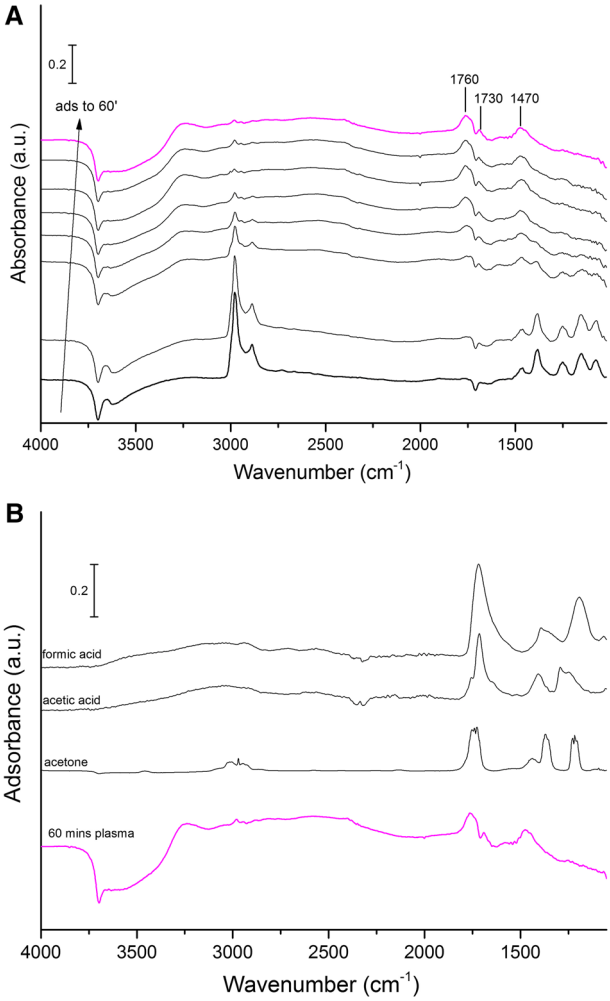

Fig. 5 DRIFT Spectra on TiO_2. **a** In situ IR spectra of the evolution of adsorbed isopropanol as a function of plasma treatment time from *bottom* to *top* (adsorbed IPA then 1, 5, 10, 20, 30, 45 and 60 min of plasma treatment). **b** Spectra of adsorbed IPA after 60 min of plasma treatment and adsorbed acetone, acetic acid and formic acid (from *bottom* to *top*)

20 min treatment and the large band at 1730 cm^{-1} was assigned to acetone formation. The small residual contribution remaining at 1150 cm^{-1} could correspond to C–O bonds stretching and assign to formic acid formation. These observations show that isopropoxide species formed by the dissociative adsorption of isopropanol give rise to acetone and formic acid on γ-Al_2O_3 when treated by non-thermal plasma under air.

On TiO_2, an increase and a broadening of the δ-as C–H band (1470 cm^{-1}) and the total disappearance of δ-s C–H band (1385 cm^{-1}), were observed as a function of the plasma treatment time. The IPA bands at lower wavenumbers: δ-O–H (1253 cm^{-1}), C–O stretching and C–C skeletal elongation (1150 and 1075 cm^{-1}), progressively weakened till complete disappearance as the plasma treatment time increased showing that IPA on TiO_2

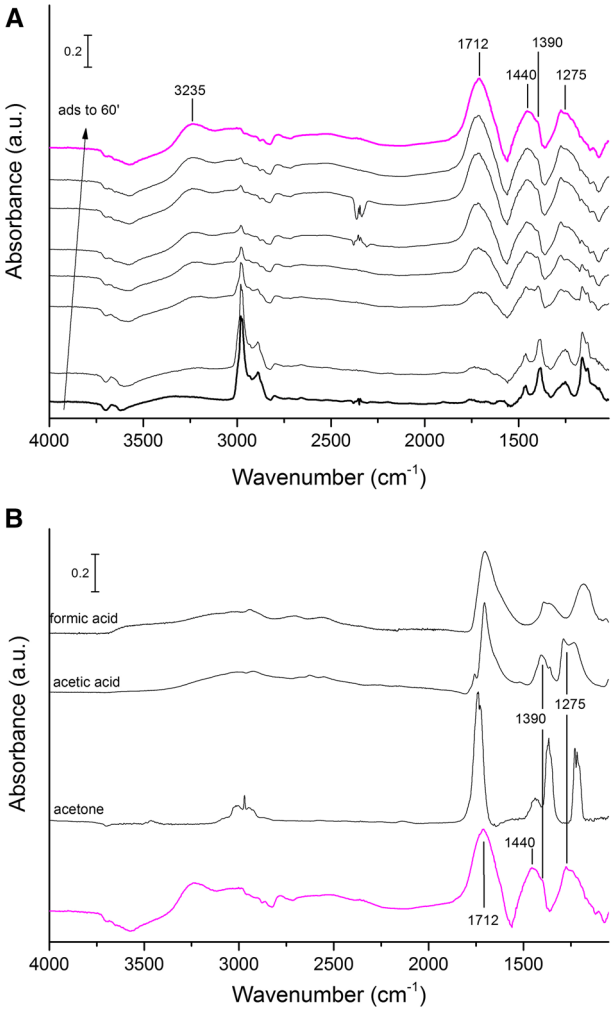

Fig. 6 DRIFT Spectra on CeO_2. **a** In situ IR spectra of the evolution of adsorbed isopropanol as a function of plasma treatment time from *bottom* to *top* (adsorbed IPA then 1, 5, 10, 20, 30, 45 and 60 min of plasma treatment). **b** Spectra of adsorbed IPA after 60 min of plasma treatment and adsorbed acetone, acetic acid and formic acid (from *bottom* to *top*)

Scheme 1 Adsorption mode of IPA (*M* metallic cation)

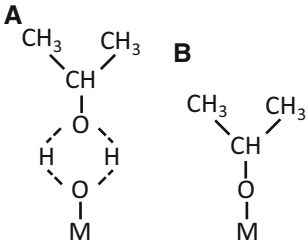

is rapidly oxidized into acetone followed by further decomposition into CO_2 and gas phase water. A small acidic residue is visible from the broad band in the 3000 cm^{-1} region. Additionally, at 1470 cm^{-1} and in smaller extend at 1590 cm^{-1} bands were identified and corresponded to the C–H bending and the COO^- stretching, respectively.

On CeO_2, the bands corresponding to the δ-as (1470 cm^{-1}) and δ-s (1390 cm^{-1}) bending mode of methyl are evolving and broadening as a function of the plasma treatment time. In the same time, a large band is growing at 1275 cm^{-1} which corresponds to the O–H bending vibration mode of carboxylic acids. As for the two other samples, it is difficult to differentiate the different acids and their contribution due to the overlapping of the bands in this region. Cerium oxide that shows particularly broad bands makes it difficult to observe the evolution of acetone formation/oxidation on this surface. Finally, an interesting feature, only visible on CeO_2 is the adsorption/desorption of CO_2 in the 2300–2400 cm^{-1} region (2365 and 2333 cm^{-1}), that may arise from the decomposition of IPA into CO_2. However, we have to be careful with this interpretation since published work on CO_2 adsorption on γ-Al_2O_3 [34] or tin oxide [35] revealed the presence of bands in the 1900–1200 cm^{-1} range relative to adsorbed CO_2, which may, in this case, be hidden by other contributions at low wavenumbers.

According to these observations, the steps following IPA stabilization on the surface can follow these two pathways: either its oxidation into acetone, either a C–C bond breakage of a methyl group. Oxidation reactions taken place here can either come from a radical attack, probably from $O^{\cdot}$ or $^{\cdot}OH$, on the –OH group of IPA, either via redox reactions of the adsorbed isopropoxide species on the metal oxide surface acid sites. C–C bond breakage can be achieved by $^{\cdot}OH$ radical attack and the resulting methyl radical can react with oxygenated species to form formaldehyde, then formic acid. The other radical fragment, $CH_3CH^{\cdot}OH$, can then be oxidized in acetaldehyde, then in acetic acid. On alumina, the formation of propene from IPA dehydration can also occurs, followed by its decomposition into CO_2 and H_2O.

Toluene Removal

The experiments regarding toluene elimination were performed in the same conditions as for IPA removal. Toluene was previously adsorbed on the catalysts (100 ppm in air for 10 min, 30 mL min^{-1}) followed by purging with dry air before the start of the plasma treatment. The recorded spectra as a function of time are presented in Fig. 7a–c. As expected, on the three oxides the main reference IR bands of adsorbed toluene are visible at around 3100–3000 cm^{-1} domain corresponding to the C–H aromatic (3030 and 3080 cm^{-1}) and at 2930 and 2880 cm^{-1} corresponding to the C–H stretching of the methyl group and at 1495, 1460 and 1610 cm^{-1}, corresponding to the C–C stretching in the aromatic ring. The negative bands at 1705 (bending mode of hydrogen bonded surface hydroxyls) and 3695 cm^{-1} (stretching mode) could be assigned to the loss of surface hydroxyl group upon toluene adsorption [36–40]. On CeO_2 and to a lesser extent on γ-Al_2O_3, a small contribution of in plane C–H bending at 1081 and 1035 cm^{-1} was identified as well as weak bands at 1160 and 1180 cm^{-1} for CeO_2 and γ-Al_2O_3, respectively. Finally, a weak overtone in the 2000–1800 cm^{-1} region is detected.

As soon as the plasma was generated, and this independently of the catalyst sample tested, the C–H aromatic bands (3030 and 3080 cm^{-1}) decreased rapidly after only 1 min of plasma treatment and this until 10 min. At 10 min, no C–H aromatic contribution is visible, and this for the three surfaces, indicating the complete transformation of toluene.

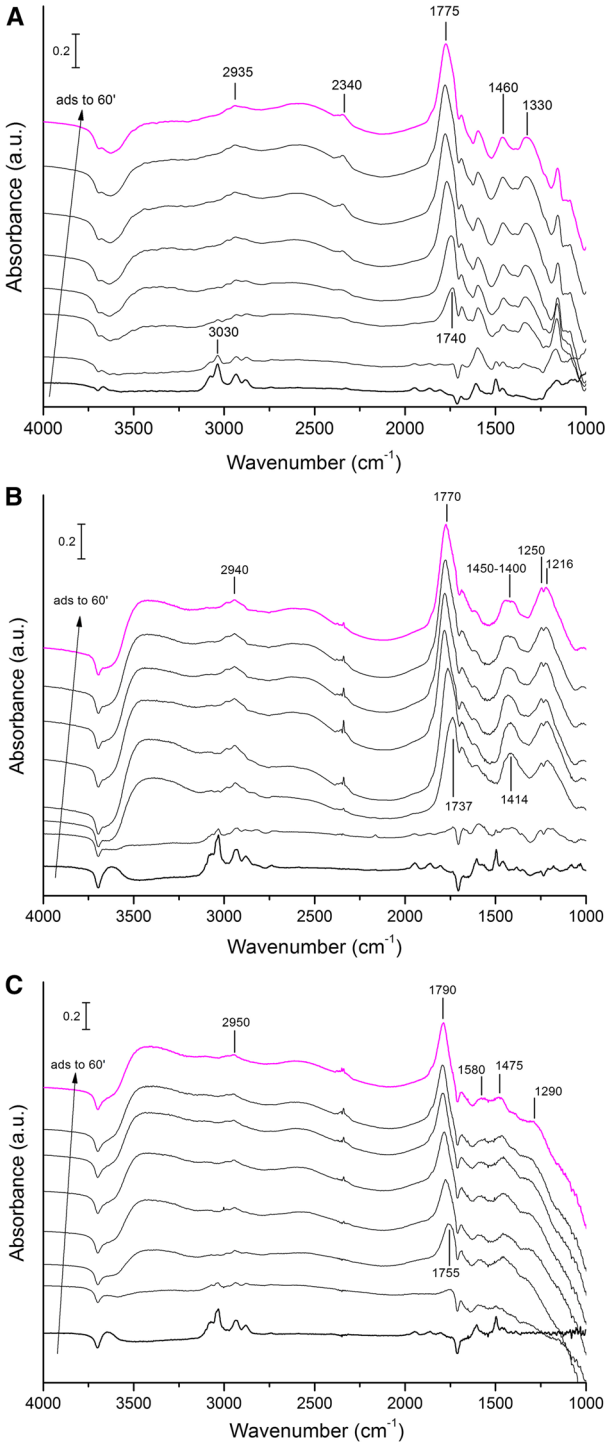

Fig. 7 In situ DRIFT spectra of the evolution of toluene on **a** γ-Al_2O_3, **b** CeO_2 and **c** TiO_2 as a function of plasma treatment time from *bottom* to *top* (adsorbed toluene then 1, 5, 10, 20, 30, 45 and 60 min of plasma treatment)

In the same time, a strong band in the 1730–1755 cm^{-1} region evolved after 5 min of plasma treatment characteristic of the presence of a C=O bond. As the plasma treatment time increased, the band increased, shifted to higher wavenumber after 10 min of plasma to reach 1775, 1770 and 1790 cm^{-1} on γ-Al_2O_3, CeO_2 and TiO_2, respectively (Table 2 and Fig. 7).

The non-symmetry of the bands and apparition of a shoulder (1700–1725 cm^{-1}) at 10 min for CeO_2 and TiO_2 and 20 min for γ-Al_2O_3 indicate the presence of a carboxylic acid in addition to aldehyde or ester [25, 41]. The bands at 1330, 1250 and 1290 cm^{-1} on γ-Al_2O_3, TiO_2 and CeO_2, respectively, can be attributed to C–O stretching. In addition, the broad shoulder of O–H stretching (2500–3500 cm^{-1}) confirms the presence of carboxylic acid. Independently of the catalyst, the growing of the 1790–1770 cm^{-1} band is associated with the formation of a negative signal in the OH vibration domain (3500–3700 cm^{-1}) showing that the species formed under plasma adsorb on OH surface groups. By increasing the plasma treatment duration, the main change is the shift of the C=O band for more than 10 min of plasma. This shift could be assigned to the formation of bridged carbonates [42] on the catalysts surface showing the total oxidation of toluene under plasma treatment.

A band at 1345 cm^{-1} appeared after 1 min and could also correspond to primary O–H bending (δ-OH) or =C–OH phenol stretching. The band increased and shifted to 1330 cm^{-1} until 20 min and remained constant until 60 min. At this wavenumber, the functional group identified is more likely C–O from carboxylic acid or =C–OH phenol stretching but also N–O symmetrical stretching from olefinic compounds. However, other nitrogen related contribution were not identified.

On CeO_2, less intense bands appear at 1414 and 1250–1216 cm^{-1} which could be due to the formation of carboxylic acids (O–H bending and C–O stretching, respectively) and at 1610 cm^{-1} which could be assigned to the formation of adsorbed formate species [43]. The relative intensity of this band decreases from γ-Al_2O_3, TiO_2 to CeO_2, following the increasing oxidative property (or basicity) of these oxides.

On the three surfaces, the band of C=C stretching at $\sim$1460 and at $\sim$1610 cm^{-1} broadened and increased until 60 min while the one at $\sim$1495 cm^{-1} decreased until complete disappearance. The increasing and broadening of the 1460 cm^{-1} band could be due to various stretching behavior such as C=C of phenol or C=C from alkenes indicating a rupture of the aromatic ring. A weak shoulder in the 2950–2930 cm^{-1} region, indicates the

Table 2 Shift of the C = O band as a function of plasma treatment time and corresponding chemical groups [25, 34]

Plasma time (min)	0	1	5	10	20	30	45	60
Wavenumber maxima (cm^{-1})								
Al_2O_3	–	1740	1740	1745	1769	1775	1775	1775
Corresponding carbonyl group		Aldehyde/ester	Ald/ester	Ald/ester	Ald/ester/acid	Carb.		
CeO_2	–	1736	1736	1760	1783	1770	1770	1770
Corresponding carbonyl group		Aldehyde/ester	Ald/ester	Ald/ester/acid	Carb.			
TiO_2	–	1750	1750	1775	1782	1790	1790	1790
Corresponding carbonyl group	–	Aldehyde/ester	Ald/ester	Ald/ester/acid	Carb.			

Ald aldehyde, *carb* carbonate

presence of C–H stretching from methyl group only, without aromatic contribution. The presence of bands in the 2300–2400 cm^{-1} domain is associated to the presence of adsorbed CO_2.

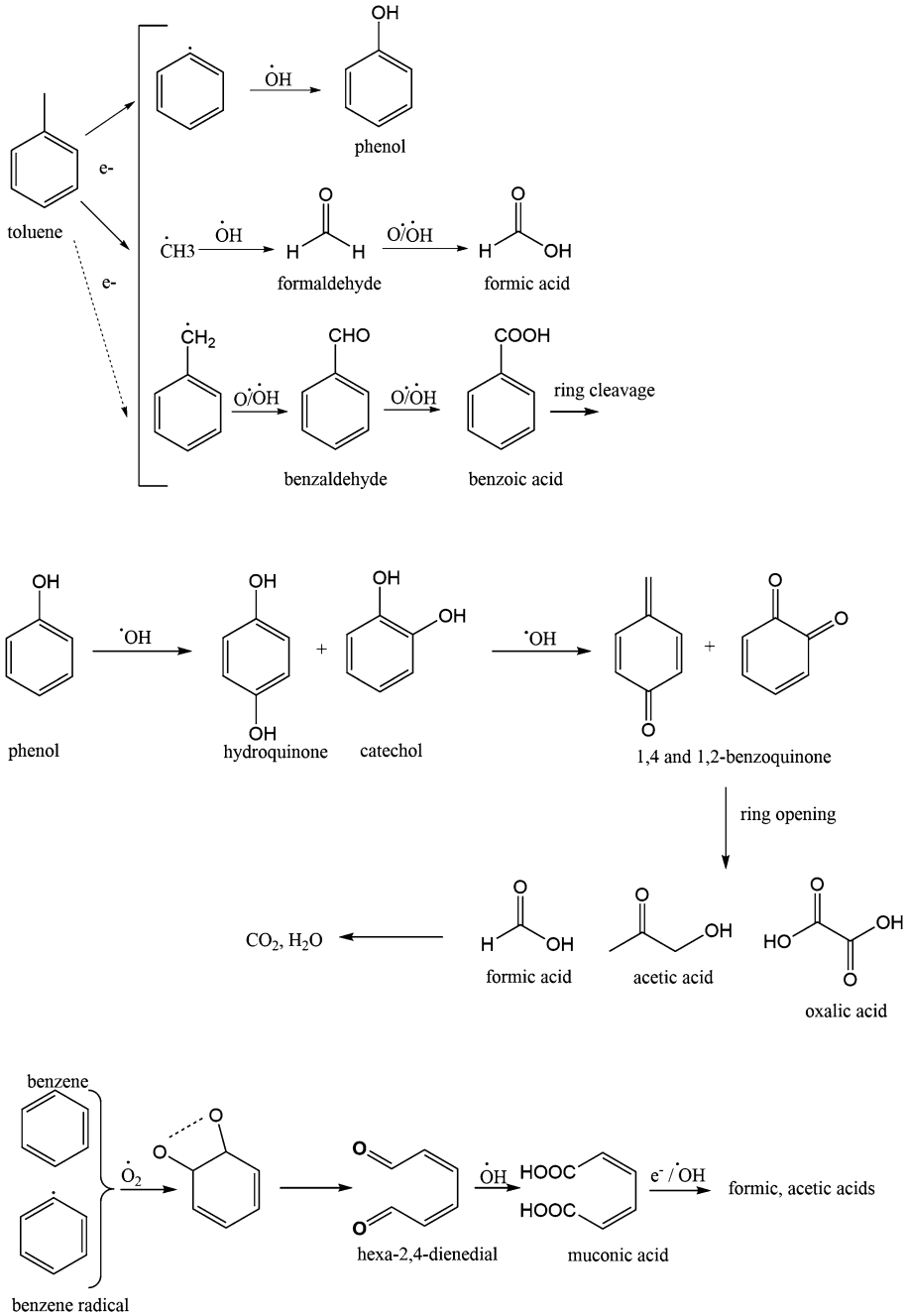

Fig. 8 Possible mechanism pathways and intermediates of toluene oxidation and degradation

According to the results of various authors [44–52] and ours, we can propose some probable reaction mechanisms for toluene elimination. First of all, Kohno et al. [44] showed that, from the three pathways undertaken by NTAP species for VOC elimination, the electron impact would be the favored one as it presents the lowest reaction rate constant in the order of 10^{-6} cm^3 s^{-1}. The two other pathways, ion collisions and radical attack ($O^{\cdot}$/$OH^{\cdot}$) would occur subsequently and contribute to toluene oxidation and ring opening reactions. The electronic impact would lead to the formation of benzene radical that would rapidly be oxidized in phenol. For the later, the aromatic cycle would be rapidly hydroxylated into hydroquinone, further oxidized in benzoquinone. Finally the ring would be opened by oxygen or OH radicals leading to the formation of aldehydes and carboxylic acids with different carbon chains length. Possible mechanisms are displayed in Fig. 8. As long as oxidative radicals are present, in addition to electronic impact, the reaction would continue until complete fragmentation into CO_2 and H_2O following various mechanisms that are currently not completely identified and still need further investigation. Additionally, methyl radical would be oxidized in formic acid followed by complete elimination in CO_2/H_2O. It seems that the oxidation of the methyl group on toluene, leading to benzaldehyde and benzoic acid, is not the favored pathway undertaken for toluene oxidation by non-thermal plasma. In fact, from our results, it seems that the band related to C=O apparition coincides with the complete disappearance of aromatic C–H bands, indicating a rapid opening of the aromatic ring prior to the oxidation of the fragments into carboxylic acid.

Conclusions

This new infrared cell allows characterizing by DRIFT the adsorbed organic species on a catalyst surface under DBD non-thermal plasma and in controlled gaseous environment at atmospheric pressure, realizing then a true operando analysis of a catalyst surface submitted to the action of a non-thermal plasma. The method has proven to be so efficient that it was possible to follow the evolution of secondary compounds, arising from the oxidation of isopropanol and toluene. The plasma treatment of IPA molecules adsorbed on γ-Al_2O_3, TiO_2 and CeO_2 surfaces led to the formation of acetone, propene, acetic acid and/or formic acid. On CeO_2 and TiO_2 surface, only acids remained after 60 min of plasma treatment while γ-Al_2O_3 showed a small presence of acetone and propene on its surface. By contrast, the toluene oxidation by non-thermal plasma led to the rapid opening of the aromatic ring, followed by the total oxidation through carboxylic formation of the species arising from the toluene molecules fragmentation. These results should be considered as preliminary experiments probing the extended possibilities of this new IR cell to characterize in operando conditions a catalyst or any surface submitted to a non-thermal plasma and are able to improve the knowledge on plasma material interactions.

Acknowledgments The authors would like to thank the French Ministry of Research for the funding of the Ph.D. Grant of A. Rodrigues.

References

1. Bogaerts A, Neyts E, Gijbels R, Van der Mullen J (2002) Spectrochim Acta B 57:609–658
2. Tendero C, Tixier C, Tristant P, Desmaison J, Leprince P (2006) Spectrochim Acta B 61:2–30

3. Kogelschatz U, Eliasson B, Egli W (1999) Pure Appl Chem 71:1819–1828
4. Van Durme J, Dewulf J, Leys C, Van Langenhove H (2008) Appl Catal B Environ 78:324–333
5. Hyun-Ha K (2004) Plasma Process Polym 1:91–110
6. Vandenbroucke AM, Morent R, De Geyter N, Leys C (2011) J Hazard Mater 195:30–54
7. Tosi P, Ascenzi D, Franceschi P, Guella G (2009) Plasma Sour Sci Technol 18:034005
8. Tanarro I, Herrero VJ (2009) Plasma Sour Sci Technol 18:034007
9. Babayan SE, Ding G, Nowling GR, Yang X, Hicks RF (2002) Plasma Chem Plasma Process 22:255–269
10. Cruden BA, Rao MVVS, Sharma SP, Meyyappan M (2003) J Appl Phys 93:5053–5062
11. Rivallan M, Aiello S, Thibault-Starzyk F (2010) Rev Sci Instrum 81:103111
12. Nakagawa Y, Ono R, Oda T (2014) IEEE Trans Ind Appl 50:39–44
13. Liao X, Guo YF, He JH, Ou WJ, Ye DQ (2010) Plasma Chem Plasma Process 30:841–853
14. Rivallan M, Fourré E, Aiello S, Tatibouët JM, Thibault-Starzyk F (2012) Plasma Process Polym 9:850–854
15. Kim HH, Teramoto Y, Negishi N, Ogata A (2015) Catal Today 256:13–22
16. Barakat C, Grajevat P, Guaitella O, Thévenet F, Rousseau A (2014) Appl Catal B Environ 147:302–313
17. Jarrige J, Vervisch P (2006) J Appl Phys 99:113303
18. Karuppiah J, Sivachandiran L, Karvembu R, Subrahmanyam CH (2010) Chem Eng J 165:194–199
19. Sivachandiran L, Thévenet F, Rousseau A (2013) Plasma Chem Plasma Process 33:855–871
20. Al-Abduly A, Christensen P (2015) Plasma Sour Sci Technol 24:065006
21. Manley TC (1943) Trans Electrochem Soc 84:83–96
22. del Arco M, Gutiérez S, Martin C, Rives V (2001) Phys Chem Chem Phys 3:119–126
23. Ermini V, Finocchio E, Sechi S, Busca G, Rossini S (2000) Appl Catal A Gen 167:157–167
24. Zaki MI, Hussein GAM, El-Ammawy HA, Mansour SAA, Polz J, Knözingze H (1990) J Mol Catal 57:367–378
25. Coates J (2000) Interpretation of infrared spectra, a practical approach. In: Mayer RA (ed) Encyclopedia of analytical chemistry, pp 10815–10837
26. Al-Abadleh HA, Grassian VH (2003) Langmuir 19:341–347
27. Devlin JP, Buch V (1997) J Phys Chem B 101:1095–1098
28. Devlin JP, Sadley J, Buch V (2001) J Phys Chem A 105:974–983
29. Narengerile, Watanabe T (2012) Chem Eng Sci 69:296–303
30. Neaţu S, Sacaliuc-Pârvulescu E, Lévy F, Pârvulescu VI (2009) Catal Today 142:165–169
31. Hasan MA, Zaki MI, Pasupulety L (2003) Appl Catal A Gen 243:81–92
32. Benaliouche F, Boucheffa Y, Thybault-Starzyk F (2012) Microporous Mesoporous Mater 147:10–16
33. Lakshmanan P, Delannoy L, Louis C, Bion N, Tatibouët JM (2013) Cat Sci Technol 3:2918–2925
34. Parkyns ND (1969) J Chem Soc A 410–417
35. Thornton EW, Harrison PG (1975) J Chem Soc, Faraday Trans 1:461–472
36. Morterra C, Ghiotti G, Garrone E, Boccuzzi F (1976) J Chem Soc, Faraday Trans 72:2722–2734
37. Lee DH, Condrate RA Sr (1995) Mater Lett 23:241–246
38. Digne M, Sautet P, Raybaud P, Euzen P, Toulhoat H (2002) J Catal 211:1–5
39. Harrison PG, Guest A (1987) J Chem Soc, Faraday Trans 83:3383–3397
40. Wachs IE (1995) Colloid Surf A 105:143–149
41. Larkin PJ (2011) IR and Raman spectroscopy: principles and spectral interpretation. Elsevier, Amsterdam
42. Little LH (1966) Infrared spectra of adsorbed species. Academic Press, New York
43. Köck EM, Kogler M, Bielz T, Klötzer B, Penner S (2013) J Phys Chem C 117:17666–17673
44. Kohno H, Berezin AA, Chang JS, Tamura M, Yamamoto T, Shibuya A, Hondo S (1998) IEEE Trans Ind Appl 34:953–966
45. Zhu T, Wan YD, Li Y, He XW, Xu DY, Shu XQ, Liang WJ, Jin YQ (2011) Int J Environ Sci Technol 8:621–630
46. Huang H, Ye D, Leung DYC, Feng F, Guan X (2011) J Mol Catal A: Chem 336:87–93
47. Xiao G, Xu W, Wu R, Ni M, Du C, Gao X, Luo Z, Cen K (2014) Plasma Chem Plasma Process 34:1033–1065
48. Klotz B, Barnes I, Becker KH, Golding BT (1997) J Chem Soc, Faraday Trans 93:1507–1516
49. An G, Sun Y, Zhu T, Yan X (2011) Chemosphere 84:1296–1300
50. Cheng HH, Chen SS, Yoshizuka K, Chen YC (2012) J Water Chem Technol 34:179–189
51. Lukes P, Locke BR (2005) J Phys D Appl Phys 38:4074–4081
52. Berndt T, Böge O (2001) Phys Chem Chem Phys 3:4946–4956